Japanese Journal of
Applied Physics

REGULAR PAPER

Automated nanotube stamping system for direct delivery of liquid substances into adherent cells

To cite this article: Riku Shibata *et al* 2025 *Jpn. J. Appl. Phys.* **64** 057001

Japanese Journal of Applied Physics **64**, 057001 (2025) **REGULAR PAPER**
https://doi.org/**10.35848/1347-4065/add3e0**

Automated nanotube stamping system for direct delivery of liquid substances into adherent cells

Riku Shibata[1], Sho Ikeda[1], Aya Fujiwara[1], Riko Kishida[1], Shota Yanagisawa[1], Shun Fukabori[1], Yuiko Mizuguchi[2], Kazuhiro Oyama[2], Takeo Miyake[2], and Takashi Tanii[1*]

[1]*Department of Electronic and Physycal System, Waseda University, Shinjuku, Tokyo 169-8555, Japan*
[2]*Graduate School of Information, Production and Systems, Waseda University, Kitakyushu, Fukuoka 808-0135, Japan*

[*]E-mail: tanii@waseda.jp

Received February 13, 2025; revised April 22, 2025; accepted May 2, 2025; published online May 21, 2025

Nanotube (NT) stamping has the advantage of delivering substances to a large number of cells in a shorter time. However, because it was controlled manually, the results varied depending on the individual performing the procedure. Here we propose an automated NT stamping system that enhances the accuracy and reproducibility of delivering liquid substances into cells by combining stepper motor control and image processing with a conventional inverted microscope. The automated system inserts NTs into adherent cells by sequential two-step focusing of the objective lens on the target cells and the NT membrane. We show that the automated system achieves submicron precision in controlling the vertical position of the NTs relative to the adherent cells by the two-step focusing while maintaining a high delivery rate of 72% and high cell viability of more than 90%. The target substances can be delivered into the nuclei of HeLa cells preferentially by our stamping system.

1. Introduction

Nanotube (NT) stamping is a technique for delivering target substances directly into cytoplasm. By inserting an array of NTs protruding from the outer bottom surface of an open-top glass cylinder into the cell membrane, liquid substances in the cylinder can diffuse into the cytoplasm (Fig. 1).[1,2] Such direct intracellular delivery techniques have potential to evaluate the effectivity of drugs or even to impart new functionalities to cells.[3–14] Thus far, the NT stamping has achieved both a high delivery rate and high cell viability. Furthermore, a variety of substances, including biomolecules, biomarkers and nanoparticles, can be delivered by NT stamping when they are dissolved or dispersed in the liquid.[1,2]

The key to achieving both a high delivery rate and high cell viability by the NT stamping is precise control of the vertical position of the NT membrane relative to adherent cells precisely. The NTs are fabricated by electroless plating of gold on a track-etched membrane and subsequent dry etching of the membrane surface.[1] Thus, the thin gold film deposited on the inner wall of pores in the track-etched membrane remains on the surface as NTs after dry etching [Fig. 1(a)]. Commonly, the NTs are fabricated so as to protrude from the membrane surface by approximately 8 μm, which is in the same order of the height of adherent cells.[15–17] Hence, the NT membrane position needs to be controlled with a submicron precision when inserting NTs into cells. If the membrane is placed apart from the cell top, the substances may be delivered to the culture medium rather than the cytosol. Contrastingly, excessively deep insertion may induce damage into the cells.

Industrial applications of NT stamping require high reproducibility for the membrane position control. An automated system has the potential to enhance processing speed as well as reproducibility. Such systems can be incorporated in the production line of artificially modified cells, such as smart cells.[7,18–26] However, so far, the vertical position of the NT membrane has been controlled by human manipulation, depending on the operator's skill.

Here, we propose an automated NT stamping system which combines image processing and stepper motor control with a conventional inverted optical microscope (Fig. 1). The open-top glass cylinder with the NT membrane as the base plate is mounted on the stepper motor while the vertical position of the NT membrane is controlled by software to capture specimen images and measure the vertical position of the specimen in real time. We demonstrate that this automated NT stamping system achieves submicron precision in control of the NT membrane position relative to the target cells, thereby improving the reproducibility of liquid substance delivery.

2. Experimental methods

2.1. Cell culture

HeLa cells were cultured in glass bottom dishes (Matsunami, 35 mϕ dish) until a confluent or sub-confluent condition was achieved. The culture process was as follows. HeLa cells were suspended in 5 ml of a culture medium containing 61.3 mg of a basic medium (Gibco, Dulbecco's modified eagle medium basic medium), 0.27 mg of penicillin, 0.45 mg of streptomycin, 16.8 mg of $NaHCO_3$, 0.45 ml of fetal bovine serum (FBS) (Gibco), 4.5 ml of ultrapure water, and 4.5 μl of hydrochloric acid at 37 °C. Then the suspension was centrifuged at 500 rpm for 4 min. After removing the supernatant fluid, the cell precipitation was mixed with 5 ml of the culture medium. Then, the suspension was centrifuged again at 500 rpm for 4 min, and the supernatant liquid was removed. Finally, the cell precipitation was mixed with a culture medium, and the cells seeded on the dish bottom were incubated in 5% CO_2 at 37 °C for approximately 2 d. Then, the cells were used for NT stamping.

2.2. Nanotube stamping with stepper motor control and image processing

We used an inverted optical microscope (Olympus, IX70) equipped with a complementary metal oxide silicon (CMOS) camera (Andor, Zyla 4.2 PLUS). Phase contrast images of the target cells as well as reflected images of the NT membrane were taken with the same objective lens (Olympus, LUCPLFLN20XPH). The correction ring of the objective

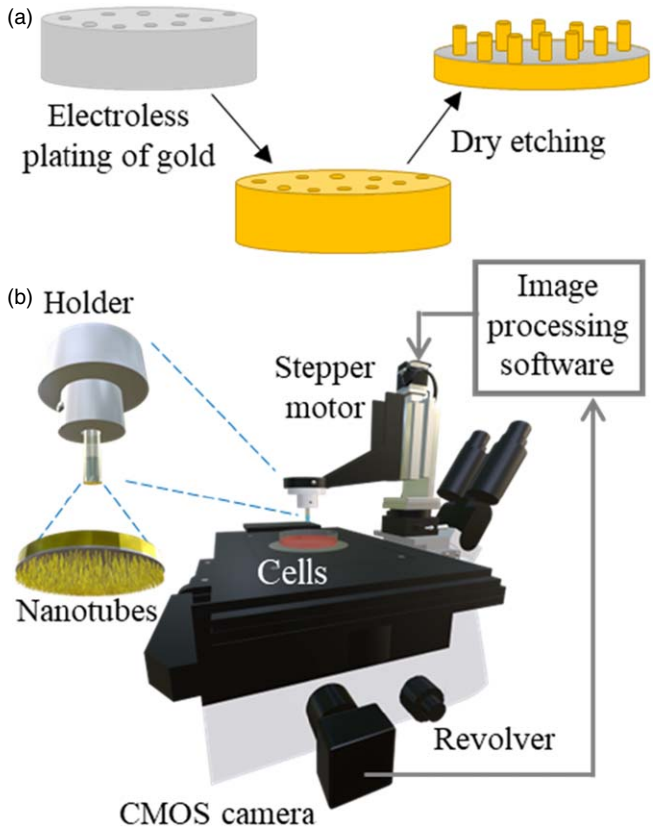

Fig. 1. Nanotube stamping system. (a) Process for fabrication of the nanotube membrane. (b) Schematic of nanotube stamping system.

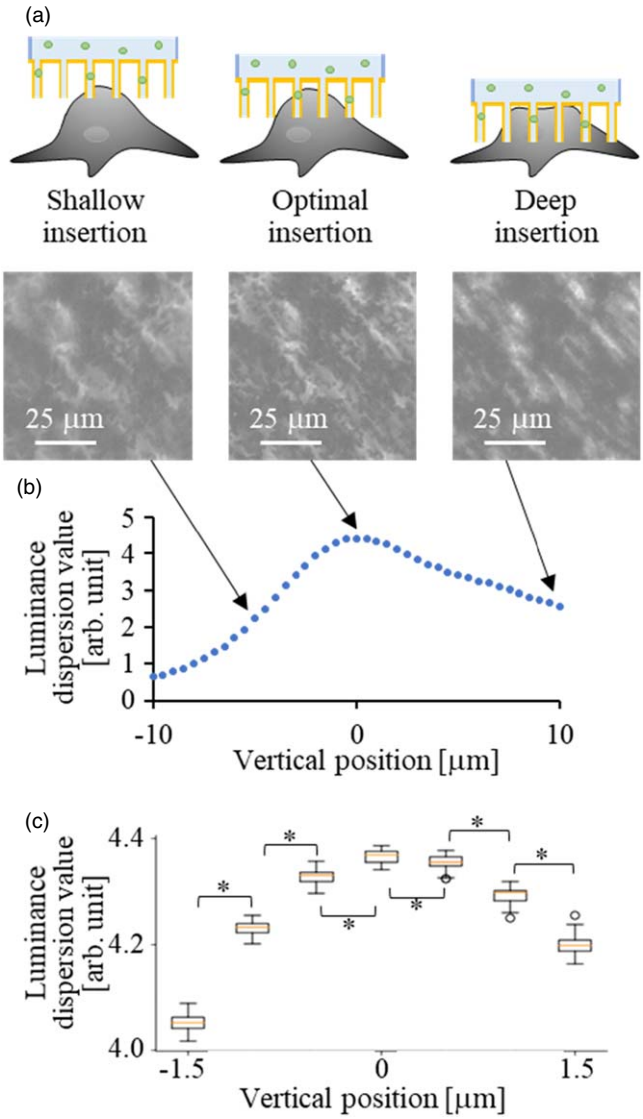

Fig. 2. Image processing software. (a) Schematic of nanotube insertion into cells and corresponding reflected images of nanotubes. (b), (c) Relationship between the vertical position of the nanotube membrane and the luminance dispersion value calculated from the reflected image of nanotubes by image processing software. *, $p < 0.05$.

lens is useful for the optical alignment of both the phase contrast and reflected light microscopy. As shown in Fig. 1(b), a stepper motor (Surugaseiki, KZG06030-GA, DS 102) for vertical movement and manual stages (Surugaseiki, B210-60CN; Chuo precision industrial, TD602) for horizontal and rotational movement with tilt angle adjustment were mounted on the microscope. The resolution of the vertical movement of the stepper motor was set to be 0.05 μm. The glass cylinder with a NT membrane was fixed to the stepper motor with a metal arm. We put 200 μl of liquid substances in the glass cylinder just before bringing the NT membrane closer to the target cells.

Images captured by the CMOS camera were processed by laboratory developed software. The image processing software works as a Laplacian filter to calculate luminance dispersion value (LDV) of the captured image. Thus, the software outputs the maximum LDV when the subject is in focus,[27,28] as shown in Figs. 2(a) and 2(b). The frame rate was set to be 67 ms per frame including the exposure time of 2 ms. First, the vertical position of the objective lens was controlled by the microscope revolver so that the target cells on the dish bottom were in focus. To make this, phase contrast images of the target cells were processed by the software in real time. The objective lens was immobilized with the revolver clamp at the position where the software outputs the maximum LDV. Next, reflected images of the NT membrane were processed by the software while bringing the NT membrane closer to the cells by using the stepper motor. The descending speed was controlled to be decreased to 0.5 μm s^{-1} as the NT membrane approached the focal point. The reflected image only showed the light reflected at the gold NTs, whereas the target cells were almost invisible. Therefore, the descent of the NT membrane was able to be stopped at the focal point of the immobilized objective lens. We conjectured that the NTs were inserted into the cells when the software output the maximum LDV because we conducted optical alignment in advance, hence both the phase-contrast and reflected optics had the same focal point. The NT membrane was kept at the focal point for 10 min to deliver the liquid substances into cells by diffusion. Finally, NTs were pulled out from cells. To prevent cells from peeling off, the pulling speed was controlled to be 0.5 μm s^{-1} by using the stepper motor control. The cells were rinsed twice with phosphate buffered saline (PBS) and incubated in the culture medium in 5% CO_2 atmosphere at 37 °C for more than 10 min.

HeLa cells applied for NT stamping were cultured with a ring-shaped polydimethylsiloxane (PDMS) template placed on the dish bottom to define the cell adhesion region. The diameter of the inner circle of the PDMS ring was 6 mm, and

HeLa cells were seeded within the ring. Thus, the cells were restricted to grow out the adhesion region. The PDMS template was removed just before NT stamping. All the HeLa cells within the adhesion region were applied for NT stamping using a NT membrane with a diameter of 8 mm.

2.3. Evaluation of substance delivery rate

The delivery rate was measured by observing HeLa cells with a confocal laser scanning microscope (Olympus, FV3000). Before observation, calcein was delivered to HeLa cells by NT stamping, and HeLa cells growing within the 1 mm diameter central area of the adhesion region were observed. We used PBS solution containing 200 μM calcein for the NT stamping. After that, we performed plasma membrane staining (Thermo Fisher scientific, CellMask Deep Red plasma membrane stains). Phase contrast and confocal fluorescent images of the HeLa cells in the same area were taken, and the three-dimensional distribution of calcein was compared to the cell membrane geometry. Wedetermined that calcein was delivered preferentially by NT stamping if calcein fluorescence within the cell was more than twice as strong as the background fluorescence in the confocal microscopy image.

2.4. Evaluation of cell viability

All the HeLa cells incubated using the PDMS template were re-plated in a 96 well plate at the density of 5.0×10^3 cells per well after stamping, and the cell viability and the population doubling level (PDL) were measured by using a cell counter (Bio-rad, TC20). The cell viability was defined as the ratio of the number of live cells on day N to the total cell number. The PDL was defined as the logarithm to base 2 of the number ratio of live cells on day N to that of day zero. The trypan-blue-stained cells were evaluated as dead cells, whereas non-stained were evaluated as live cells.

3. Results and discussion

First, we investigated the accuracy of the vertical membrane position control using our automated NT stamping system. The accuracy was evaluated through the following two steps. In the first step, we assessed how precisely the focal point of the objective lens could be positioned on the target cells in the culture dish by using the microscope revolver. Specifically, we captured the phase contrast images of target cells and defined the focal point as the vertical position at which the image processing software output the maximum LDV for the phase contrast image. In the second step, we examined how accurately the NT membrane could be brought to this focal point by using the stepper motor. For this, we captured the reflected light images of gold NTs on the membrane and defined the focal point as the vertical position at which the image processing software output the maximum LDV for the reflected light image. In the final step, we retract the NTs from the cells by moving the NT stamp upward (i.e. in the negative z-axis direction) by using the stepper motor. In this paper, we define movement away from the cells as negative and deeper insertion into the cells as positive.

During the first step, the objective lens was brought closer to the target cells by the microscope revolver while monitoring the phase contrast image, stopping at the LDV peak (i.e. when the cells were in focus). This procedure was repeated 75 times, and the stop position was measured by referring to the revolver scale. The standard error of the stop position was 0.59 μm.

For the second step, we used the stepper motor to move the NT membrane toward the focal point, monitoring the reflected light image of the NTs. We then stopped the membrane's descent at the LDV peak. This procedure was repeated 75 times, and the stop position was measured by referring to the stepper motor movement, yielding the standard error of 0.67 μm. Throughout the second evaluation, the objective lens hence the focal point was fixed. If we consider that the first and second steps are performed in series, the fluctuation is convoluted to be 0.89 μm.

In addition to these evaluations, we also evaluated the accuracy of the LDV output from the image processing software itself. The LDV always fluctuated even when imaging a static specimen under the same optical conditions. To evaluate the fluctuation quantitatively, we placed the NT membrane at the focal point and captured 75 continuous images for 5 s at the frame rate of 15 frames per second. Figure 2(c) shows the relationship between the vertical position of the NT membrane and the LDV calculated from the reflected image of NTs. The standard errors with the same degree were obtained when we observed different positions of the NT membrane by reflected light microscopy or the target cells by phase contrast microscopy. Since the specimen was immobilized under the same optical condition, the error was attributed to the shot noise of the CMOS camera.[29] This shot noise can be reduced by averaging LDVs of multiple images or increasing the exposure time longer than 2 ms. Nevertheless, as shown in Fig. 2(c), there is a significant difference between the LDV at the focal point and that at the position 0.5 μm above or below it, which aligns well with the accuracy of our two-step focusing procedure. In addition, the 67 ms per frame rate provides enough duration to calculate the LDV by the image processing software and to stop the descent of the NT membrane after exposure.

The ideal resolution of the image processing in the optical axis direction is theoretically calculated to be 0.38 μm, which is equivalent to the focus depth of the objective. However, the standard error obtained in the first and second steps exceed the ideal resolution. We conjecture that the discrepancy contains the error in controllability of the machinery such as the revolver and the stepper motor. Nevertheless, the precision of the stepper motor control and the image processing is confirmed to be less than 1.0 μm experimentally.

Next, we evaluated the delivery rate of substances to target cells. To do this, we delivered cell-impermeable fluorescent molecules, calcein, to HeLa cells, and analyzed three-dimensional images obtained by confocal laser scanning microscopy. We then calculated the total fluorescence intensity from calcein inside the cell membrane by taking multiple cross-sectional fluorescent images of calcein and the cell membrane. Thus, non-specific adsorption of calcein on the outside of the cell membrane and the background fluorescence from other molecules outside the cell membrane were excluded from the total fluorescence intensity. We concluded that calcein had been delivered into the cells if the ratio of the total fluorescence intensity from calcein inside the cell membrane to the average background fluorescence intensity reached at least twice as strong as the background

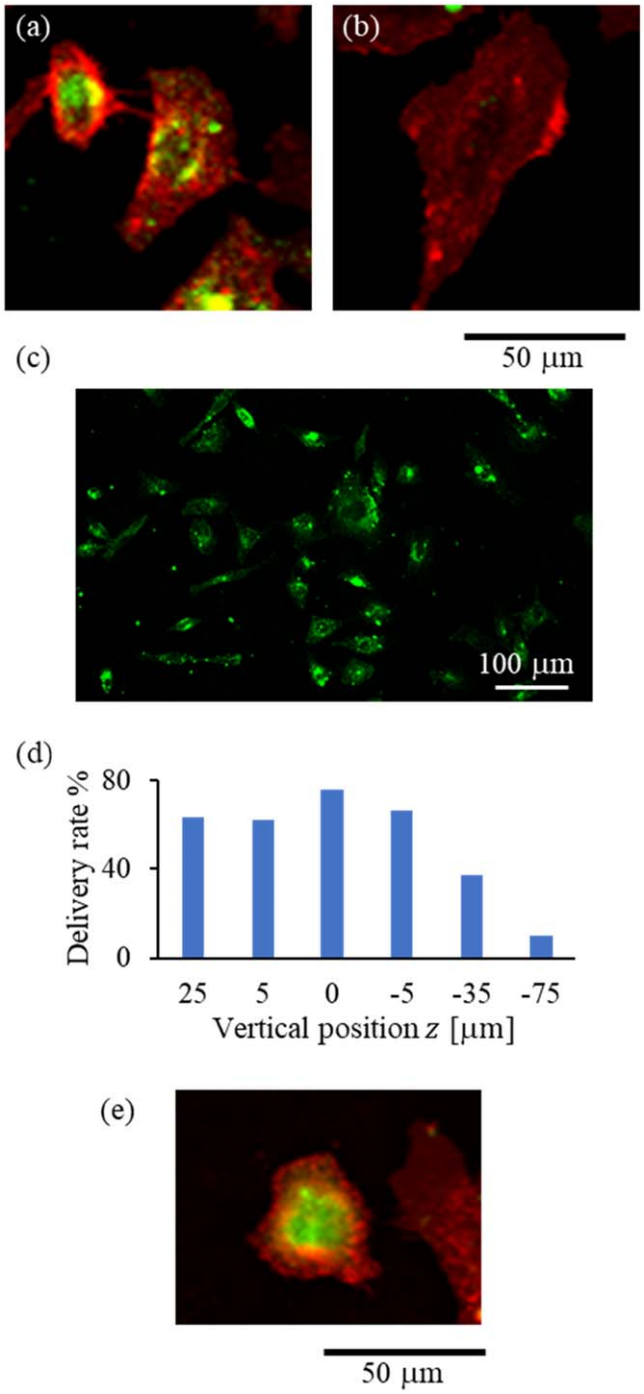

Fig. 3. Calcein delivery into HeLa cells with automated nanotube stamping system. Confocal laser scanning microscopy images of calcein (green) and plasma membrane staining (red) on cells when the nanotube membrane was placed at the focal point ($z = 0$ μm) (a) and at 75 μm above the focal point ($z = -75$ μm) (b). (c) Confocal laser scanning microscopy image of cells after calcein delivery. The central area (1mm × 1mm.) after nanotube stamping was observed individually with the image. (d) Relationship between the vertical position of the nanotube membrane and the delivery rate. (e) Confocal laser scanning microscopy image showing that calcein is delivered into nucleus.

level. In addition, we placed the NT membrane 75 μm above the focal point ($z = -75$ μm) as a reference (i.e. no NT insertion). As shown in Fig. 3, fluorescence from calcein was observed clearly within the target cells when the NT membrane was placed at the focal point ($z = 0$ μm). When the NT membrane was placed at the focal point, the delivery rate was 72%, higher than the delivery rates at other vertical positions. The increase in delivery rate from $z = -75$ μm to $z = -35$ μm is due to the fluctuation in the height of the adherent cells, whereas the gradual decrease from $z = 0$ μm to $z = 25$ μm is attributed to the deflection of the NT membrane, which brought the NTs into contact with the culture dish surface and prevented diffusion of the liquid substances into the cells. The delivery rate at $z = -75$ μm was not zero even though the NTs were not inserted into the target cells. We conjecture that calcein diffused into cells through their damaged cell membrane.[30)]

Intriguingly, calcein was delivered dominantly to the nucleus of HeLa cells when the NT membrane was placed at near the focal points as shown in Fig. 3(e). This tendency is also observed in many cells, as shown in Figs. 3(a) and 3(c). Commonly, nuclei are in the center of the cell, suggesting that controlling the NT membrane in the center of the cell height made such delivery possible. The vertical position control of NT membrane at the submicron level by our system is effective for direct delivery into nucleus.

Figure 4 shows cell viability and the PDL after NT stamping. Again, we used $z = -75$ μm as the reference condition (no NT insertion). There is no significant difference among all the conditions including the reference. The decrease in the cell viability on day 5 is because the cell culture became confluent, hence the number of dead cells increased. However, at $z = 25$ μm, we found that NT stamping peeled off a part of the target cells, indicating that deep insertion may lift off the target cells. In short, preferential NT stamping can be performed when the NT

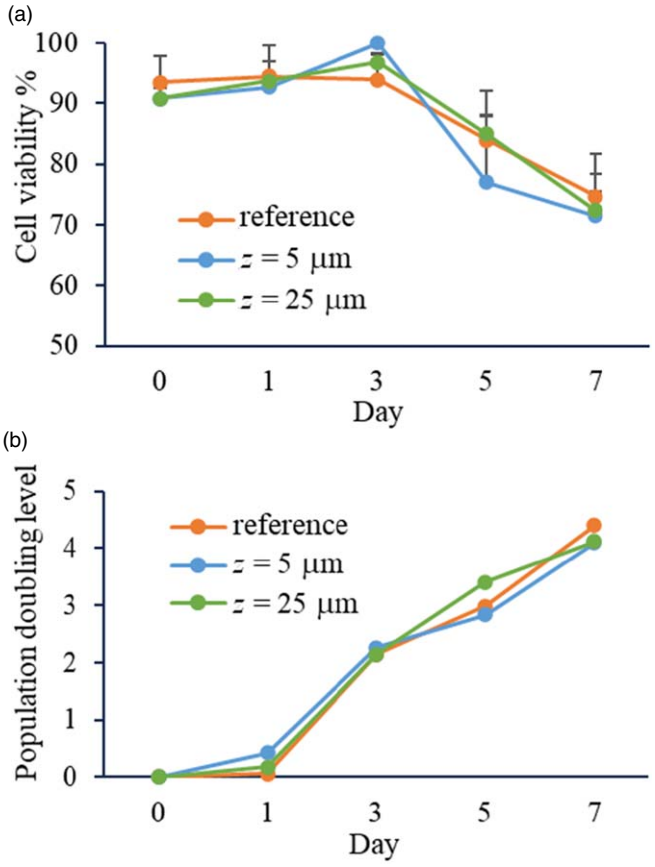

Fig. 4. (a) Cell viability and (b) population doubling level of the cells after nanotube stamping with the vertical position of the nanotube membrane as the parameter.

membrane is kept at the focal point by using the stepper motor control and the image processing.

4. Conclusion

We proposed an automated NT stamping system to enhance the accuracy and reproducibility of liquid substance delivery into adherent cells. This system combines stepper motor control and image processing with a conventional optical microscope, achieving a standard error of 0.89 μm in the vertical positioning of the NT membrane. Moreover, cell viability remained intact after NT stamping. Although the objective lens was controlled manually with the microscope's revolver in our setup, the standard error in its vertical positioning could similarly be minimized to a submicron level, as demonstrated by the NT membrane control. In summary, the proposed system achieves submicron accuracy and reproducibility for liquid substance delivery into adherent cells.

Acknowledgments

This work was supported by JSPS KAKENHI Grant No. 24H02333, and partly by "Advanced Research Infrastructure for Materials and Nanotechnology in Japan (ARIM)" and "Design & Engineering by Joint Inverse Innovation for Materials Architecture (DEJI2MA Project)" of the Ministry of Education, Culture, Sports, Science and Technology (MEXT). Additionally, this work was partly funded by the Japan Science and Technology Agency (JST) under the PRESTO program, Grant No. JPMJPR20B8 and JST SCORE University Promotion Type Grant No. JPMJST2053, awarded to T. Miyake.

1) B. Zhang, Y. Shi, D. Miyamoto, K. Nakazawa, and T. Miyake, Sci. Rep. **9**, 6806 (2019).
2) B. Zhang, B. Liu, Z. Wu, K. Oyama, M. Ikari, H. Yagi, N. Tochio, T. Kigawa, T. Mikawa, and T. Miyake, Anal. Chem. **96**, 8349 (2024).
3) R. Wen et al., ACS Appl. Mater. Interfaces **11**, 43936 (2019).
4) C. B. Fox, Y. Cao, C. L. Nemeth, H. D. Chirra, R. W. Chevalier, A. M. Xu, N. A. Melosh, and T. A. Desai, ACS Nano **10**, 5873 (2016).
5) B. Ekwall and A. Johansson, Toxicol. Lett. **5**, 299 (1980).
6) T. Mizutani, T. Kondo, S. Darmanin, M. Tsuda, S. Tanaka, M. Tobiume, M. Asaka, and Y. Ohba, Clinical Cancer Res. **16**, 3964 (2010).
7) X. Xie, A. M. Xu, S. Leal-Ortiz, Y. Cao, C. C. Garner, and N. A. Melosh, ACS Nano **7**, 4351 (2013).
8) Y. Cao, E. Ma, S. Cestellos-Blanco, B. Zhang, R. Qiu, Y. Su, J. A. Doudna, and P. Yang, Proc. Natl. Acad. Sci. **116**, 7899 (2019).
9) D. Kim et al., Cell Stem Cell **4**, 472 (2009).
10) A. M. Xu, D. S. Wang, P. Shieh, Y. Cao, and N. A. Melosh, Chem. Bio. Chem. **18**, 623 (2017).
11) C. A. Pinkert, M. H. Irwin, L. W. Johnson, and R. J. Moffatt, Transgenic Res. **6**, 379 (1997).
12) M. Hashimoto and T. Takemoto, Sci. Rep. **5**, 11315 (2015).
13) E. Hebisch, M. Hjort, D. Volpati, and C. N. Prinz, Small **17**, 2006421 (2021).
14) Y. Cao, H. Chen, R. Qiu, M. Hanna, E. Ma, M. Hjort, A. Zhang, R. S. Lewis, J. C. Wu, and N. A. Melosh, Sci. Adv. **4**, eaat8131 (2018).
15) J. Zheng, C. Zuo, P. Gao, and G. U. Nienhaus, Opt. Lett. **43**, 5689 (2018).
16) M. Penedo, K. Miyazawa, N. Okano, H. Furusho, T. Ichikawa, M. S. Alam, K. Miyata, C. Nakamura, and T. Fukuma, Sci. Adv. **7**, eabj4990 (2021).
17) A. J. Lee, D. Yoon, S. Han, H. Hugonnet, W. Park, J.-K. Park, Y. Nam, and Y. Park, Biomed. Opt. Express **12**, 6928 (2021).
18) M. G. Aucoin, M. Perrier, and A. A. Kamen, Biotechnol. Adv. **26**, 73 (2008).
19) J. C. Grieger, S. M. Soltys, and R. J. Samulski, Mol. Ther. **24**, 287 (2016).
20) J. Alzubi et al., Mol. Ther. Methods Clinical Dev. **20**, 379 (2021).
21) P. Mukherjee, C. A. Patino, N. Pathak, V. Lemaitre, and H. D. Espinosa, Small **18**, 2107795 (2022).
22) S. Konagaya, T. Ando, T. Yamauchi, H. Suemori, and H. Iwata, Sci. Rep. **5**, 16647 (2015).
23) R. Yang, V. Lemaître, C. Huang, A. Haddadi, R. McNaughton, and H. D. Espinosa, Small **14**, 1702495 (2018).
24) C. Priesner et al., Hum. Gene Ther. **27**, 860 (2016).
25) U. Mock et al., Cytotherapy **18**, 1002 (2016).
26) D. Lock et al., Hum. Gene Ther. **28**, 914 (2017).
27) S. Paris, S. W. Hasinoff, and J. Kautz, Commun. ACM **58**, 81 (2015).
28) W. Park, I. Abramov, T. J. On, Y. Xu, A. L. Castillo, N. I. Gonzalez-Romo, R. Guckler, and M. C. Preul, Front Surg **11**, 1418679 (2024).
29) K. Wei, Y. Fu, Y. Zheng, and J. Yang, IEEE Trans. Pattern Anal. Mach. Intell. **44**, 8520 (2022).
30) Y. Zhang, X. Chen, C. Gueydan, and J. Han, Cell Res. **28**, 9 (2018).